Structural Engineering and Mechanics, Vol. 15, No. 4 (2003) 415-436
DOI: http://dx.doi.org/10.12989/sem.2003.15.4.415

Nonlinear analysis of cable-stayed spatial latticed structures

Dai Zhou† and Hongyu Liu‡

Shanghai Jiaotong University, Shanghai 200030, P.R. China

Bo Jin†

Department of Engineering Mechanics and Technology, Tongji University, Shanghai 200092, P.R. China

(Received June 25, 2002, Accepted February 25, 2003)

Abstract. The combination of spatial latticed structures (hereafter SLS) and flexible cables, the cable-stayed spatial latticed structures (hereafter CSLS) can cross longer span. According to variation principle, a novel geometric nonlinear formulation for 3-D bar elements considering large displacement and infinitesimal rotation increments with second-order precision is developed. The cable nonlinearity is investigated and it is taken that the secant modulus method can be considered as an exact method for a cable member. The tower column with which the cables link is regarded as a special kind of beam element, and, a new simplified stiffness formulation is presented. The computational strategies for the nonlinear dynamic response of structures are given, and the ultimate load carrying capacities and seismic responses are analyzed numerically. It is noted that, compared with corresponding spatial latticed shells, the cable-stayed spatial latticed shells have more strength and more stiffness, and that the vertical seismic responses of both CSLS and CLS are remarkably greater than the horizontal ones. In addition, the computation shows that the stiffness of tower column influences the performance of CSLS to a certain extent and the improvement of structural strength and stiffness of CSLS is relevant not only to cables but also to tower columns.

Key words: spatial latticed structures; cable; tower column; non-linearity; ultimate load carrying capacity; seismic response.

1. Introduction

The long-span spatial latticed structures have been fully developed around the world in the past several decades and they are good candidates for future applications due to their aesthetically attractive shape, low cost, light weight and high stiffness (Makowski 1993, Dong *et al*. 2000). Since the single structural type can not meet the need of longer span and greater variety of shapes for buildings, the hybrid spatial structures come into being, in which the disadvantages of one basic structural type are compensated with the advantages of another basic structural type. Thus, the

† Professor, Dr.
‡ Associate Professor

advantages of different basic structures can be fully utilized. Hybrid structures are formed in two ways (Kneen 1993, Schueler 1983): One is the combination among stiff structural types such as arch-truss structures; the other is the combination among flexible cables and stiff structural types, which has more wide-ranging prospects. As a flexible member, the cable can be combined with different kinds of stiff structures in several ways. For example, if the two ends of a tensed cable are fixed at two joints in a truss structure, the pre-stress truss system is formed. If the upper end of a cable is fixed on tower column and the lower end is anchored to the joint of spatial latticed structure (Dong *et al*. 2000), the CSLS can be obtained. CSLS which consists of 3-D bar element, cable member and tower column member has a few unique characteristics. Firstly, it makes full use of the high strength of steel cables. Secondly, the member's stress and deformation in structures could be controlled and sufficient structural rigidity can be provided due to the additional bearing points offered by tensioned cables. Thirdly, CSLS with its expanded impression of space may enhance the internal space and provide a landscape feature for long-span buildings. For spatial latticed structures together with cables, in a word, the strength, stiffness and stability can be improved, longer span can be obtained and the steel consumption can be reduced significantly. The use of cables as structural members in long-span structure systems is, in fact, increasing in many nations (Hosozawa *et al.* 1999).

Up to now, CSLS had also been used in many buildings in China. The roof structure of gymnasium in National Olympic Sports Center in Beijing is a combination of two cylindrical spatial latticed shells composed of the configuration of diagonal square pyramids. These two shells are connected to a spatial truss along the ridge to form a gable roof. Two tower columns are set up at both ends of the building, suspended with single directional cables. This gymnasium was completed in 1988, covering an area of 70 m × 83.2 m. CSLS was also applied to Jiuguan toll-station of Taijiu express highway in Shanxi province of China in 1995. Two separate cylindrical spatial latticed shells consisting of the configuration of orthogonal square pyramids are hung by 28 multi-directional cables from a single tower column between the two shell structures, covering an area of 14.0 m × 41.518 m. The longer span structures (over 250 m) by use of CSLS will be demanded in China in the near future.

Many publications regarding the static and dynamic analysis of spatial latticed structures can be found (Liew *et al*. 1997, Yamashita and Kato 2001, Kato and Niho 2000, Kato *et al*. 2000, Hsiao and Chang 1991, Kato *et al*. 1997, Abrate and Sun 1983, Kato and Mukaiyama 1995) in the literature. The cable dynamics and its free vibration analysis are also studied in closed form by considering the catenary profile and cable's self-weight and damping (Kim and Chang 2001, Hobbs and Raoof 1996, Starossek 1991). Some investigations on cable-supported structures were carried out to a certain extent (Krishna 2001, Buchholdt 1999, Schrefler and Odorizz 1983). So far, the literature concerning the on-going research on the behavior and properties of cable-stayed spatial latticed structures, however, is rather insufficient and further study should be made. On the other hand, It will be useful to use the research achievements in the field of long-span cable-stayed bridges for reference, because of the structural similarity. This study is focused on the nonlinear analysis of long-span CSLS.

2. Nonlinear analysis of 3-D bar element

2.1 Geometrically nonlinear analysis

We know that different formulations for 3-D beam element or 3-D bar element have been

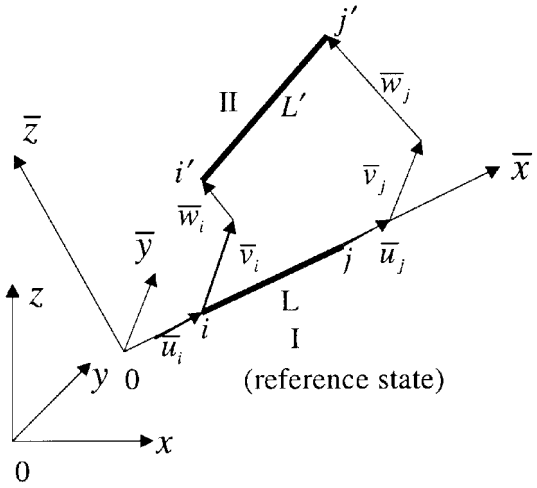

Fig. 1 The schematic diagram of an element's movement

developed to analyze the mechanical behaviors of spatial latticed shells in last decades (Schrefler and Odorizz 1983, Narayanan and Krishnamoorthy 1990, Chan 1992, Borri and Hufendiek 1985). In this study, however, a novel approach to the derivation of geometric nonlinear formulation for 3-D bar element with large displacement increments is presented. In Fig. 1, $o\overline{xyz}$ and *oxyz* are the local coordinate systems (LCS) for an element, and, global coordinate systems (GCS) for structure system respectively, and *ij* is a 3-D bar element with initial length of *L*. Define the state (I) as the initial state before deformation and the state (II) as the working state under application of load. While the structure is loaded, the element moves from the location *ij* to *i'j'*. Define the nodal displacement vector and nodal loading vector of this element as $\boldsymbol{u}_i$, $\boldsymbol{u}_j$ and $\boldsymbol{f}_i$, $\boldsymbol{f}_j$ under LCS, and as $\boldsymbol{U}_i$, $\boldsymbol{U}_j$ and $\boldsymbol{F}_i$, $\boldsymbol{F}_j$ under GCS respectively, we have

$$\left.\begin{aligned} \boldsymbol{u}_i &= [\overline{u}_i \ \ \overline{v}_i \ \ \overline{w}_i]^T, \qquad \boldsymbol{u}_j = [\overline{u}_j \ \ \overline{v}_j \ \ \overline{w}_j]^T \\ \boldsymbol{f}_i &= [f_{\overline{x}_i} \ \ f_{\overline{y}_i} \ \ f_{\overline{z}_i}]^T, \qquad \boldsymbol{f}_j = [f_{\overline{x}_j} \ \ f_{\overline{y}_j} \ \ f_{\overline{z}_j}]^T \end{aligned}\right\}$$

$$\left.\begin{aligned} \boldsymbol{U}_i &= [u_i \ \ v_i \ \ w_i]^T, \qquad \boldsymbol{U}_j = [u_j \ \ v_j \ \ w_j]^T \\ \boldsymbol{F}_i &= [F_{xi} \ \ F_{yi} \ \ F_{zi}]^T, \qquad \boldsymbol{F}_j = [F_{xj} \ \ F_{yj} \ \ F_{zj}]^T \end{aligned}\right\}$$

$$\left.\begin{aligned} \boldsymbol{u} &= [\boldsymbol{u}_j \ \ \boldsymbol{u}_i]^T, \qquad \boldsymbol{f} = [\boldsymbol{f}_j \ \ \boldsymbol{f}_i]^T \\ \boldsymbol{U} &= [\boldsymbol{U}_j \ \ \boldsymbol{U}_i]^T, \qquad \boldsymbol{F} = [\boldsymbol{F}_j \ \ \boldsymbol{F}_i]^T \end{aligned}\right\}$$

2.1.1 Geometrically nonlinear equilibrium equation in the form of work done or energy

The total potential energy Π of a 3-D bar element under state (II) is the sum of the deformation energy and the external work done by the forces (Hangai 1981),

$$\Pi = \Pi^{(i)} + \Pi^{(e)} = \frac{EA}{2}\int_0^l \varepsilon^2 dx - \boldsymbol{F}^{\boldsymbol{T}}\boldsymbol{U} \tag{1}$$

where

$$\varepsilon = \frac{L' - L}{L} = \frac{L'}{L} - 1 \tag{2}$$

E and A are the Young's modulus and the sectional area, and L and L' are the element's length at the state (I) and state (II) respectively.

Deploying the strain ε of the state (II) in the state (I) according to Taylor formulation and paying attention to $B_{(I)} = \varepsilon_{(I)} = 0$, we obtain

$$\varepsilon^2 = B + 2 - 2\sqrt{1+B} \approx \frac{1}{4}B^2 - \frac{1}{8}B^3 \tag{3}$$

where

$$B = a^2 + b^2 + c^2 + 2a \tag{4}$$

$$a = \frac{\overline{u}_j - \overline{u}_i}{L}, \quad b = \frac{\overline{v}_j - \overline{v}_i}{L}, \quad c = \frac{\overline{w}_j - \overline{w}_i}{L} \tag{5}$$

Substituting Eq. (3) into Eq. (1), the expression of the total potential energy becomes

$$\Pi = \frac{EAL}{2}\left[a^2 + a(b^2 + c^2) + \left(-\frac{5}{4}a^4 + \frac{1}{4}b^4 + \frac{1}{4}c^4\right) + \frac{1}{2}(b^2c^2 - a^2b^2 - a^2c^2)\right] + \Pi^{(e)} \tag{6}$$

The coordinate transformation for an element from GCS to LCS can be carried out according to the following processes. First, a certain rotation of GCS around the axis z is done to make the axis x coincide with the intersecting line of plane x-y and plane $\overline{x} - z$, which also make axis $\overline{y}$ at its final position. Next, another rotation of GCS around the axis y (the same as axis $\overline{y}$) makes axis $\overline{x}$ and $\overline{z}$ at their final positions respectively. Thus, the coordinate transformation matrix for an element between GCS and LCS is as follows

$$\boldsymbol{t} = \begin{bmatrix} l & m & n \\ \dfrac{-m}{\alpha} & \dfrac{l}{\alpha} & 0 \\ \dfrac{-ln}{\alpha} & \dfrac{-mn}{\alpha} & \alpha \end{bmatrix}, \qquad \alpha = \sqrt{l^2 + m^2} \tag{7}$$

where l, m and n are direction cosines of the element ij about axis x, y and z under GCS respectively. If the element ij is perpendicular to the horizontal plane, the coordinate transformation matrix is given by

$$\boldsymbol{t} = \begin{bmatrix} 0 & 0 & n \\ 0 & -n & 0 \\ 1 & 0 & 0 \end{bmatrix} \tag{8}$$

The displacement vector under LCS can be expressed by that under GCS as

$$\boldsymbol{u} = \begin{Bmatrix} \boldsymbol{u}_j \\ \boldsymbol{u}_i \end{Bmatrix} = \begin{bmatrix} \boldsymbol{t} & 0 \\ 0 & \boldsymbol{t} \end{bmatrix} \cdot \boldsymbol{U} = \begin{bmatrix} \boldsymbol{t} & 0 \\ 0 & \boldsymbol{t} \end{bmatrix} \cdot \begin{Bmatrix} \boldsymbol{U}_j \\ \boldsymbol{U}_i \end{Bmatrix} \tag{9}$$

Differentiating with respect to Eq. (6) which Eq. (9) is substituted into and making it be zero, we obtain the following nonlinear equilibrium equation

$$\frac{\partial \Pi}{\partial \boldsymbol{U}} = \frac{\partial \Pi^{(i)}}{\partial \boldsymbol{U}} + \frac{\partial \Pi^{(e)}}{\partial \boldsymbol{U}} = 0 \tag{10}$$

or

$$\begin{bmatrix} \boldsymbol{J} \\ -\boldsymbol{J} \end{bmatrix} \cdot \boldsymbol{G} = \boldsymbol{F} \tag{11}$$

$$\boldsymbol{J} = \begin{bmatrix} \frac{\partial a}{\partial u_j} & \frac{\partial b}{\partial u_j} & \frac{\partial c}{\partial u_j} \\ \frac{\partial a}{\partial v_j} & \frac{\partial b}{\partial v_j} & \frac{\partial c}{\partial v_j} \\ \frac{\partial a}{\partial w_j} & \frac{\partial b}{\partial w_j} & \frac{\partial c}{\partial w_j} \end{bmatrix} = \frac{1}{L} \begin{bmatrix} l & \frac{-m}{\alpha} & \frac{-ln}{\alpha} \\ m & \frac{l}{\alpha} & \frac{-mn}{\alpha} \\ n & 0 & \alpha \end{bmatrix} \tag{12}$$

$$\boldsymbol{F} = \frac{\partial \Pi^{(e)}}{\partial \boldsymbol{U}} = \begin{Bmatrix} \boldsymbol{F}_j \\ \boldsymbol{F}_i \end{Bmatrix} \tag{13}$$

$$\boldsymbol{G} = \begin{bmatrix} \frac{\partial \Pi^{(i)}}{\partial a} \\ \frac{\partial \Pi^{(i)}}{\partial b} \\ \frac{\partial \Pi^{(i)}}{\partial c} \end{bmatrix} = \boldsymbol{G}_1 + \boldsymbol{G}_2 + \boldsymbol{G}_3 + \ldots + \boldsymbol{G}_r + \ldots + \boldsymbol{G}_N \tag{14}$$

$$\boldsymbol{G}_1 = \frac{EAL}{2}[2a \;\; 0 \;\; 0]^T \quad \text{(linear term)} \tag{15a}$$

$$\boldsymbol{G}_2 = \frac{EAL}{2}[b^2 + c^2 \;\; 2ab \;\; 2ac]^T \quad \text{(the second-order term)} \tag{15b}$$

$$\boldsymbol{G}_3 = \frac{EAL}{2}\begin{Bmatrix} -5a^3 - 2ab^2 - 2ac^2 \\ b^3 + bc^2 - 2a^2 b \\ c^3 + b^2 c - 2a^2 c \end{Bmatrix} \quad \text{(the third-order term)} \tag{15c}$$

$$\vdots$$

$$\boldsymbol{G}_r$$

$$\vdots$$

Substituting Eq. (15a) and Eq. (15b) into the left side of Eq. (11) and introducing Eq. (12), the linear terms and the second-order terms for the element stiffness matrix are obtained respectively. Then, geometrically nonlinear equilibrium equation corresponding to accumulative displacements for 3-D bar element is as follows

$$\boldsymbol{K}_b \cdot \begin{Bmatrix} \boldsymbol{U}_j \\ \boldsymbol{U}_i \end{Bmatrix} = \begin{bmatrix} \boldsymbol{F}_j \\ \boldsymbol{F}_i \end{bmatrix} \tag{16a}$$

or

$$\boldsymbol{K}_b \cdot \boldsymbol{U} = \boldsymbol{F} \tag{16b}$$

in which

$$\boldsymbol{K}_b = \boldsymbol{K}_{1,b} + \boldsymbol{K}_{2,b} \tag{17a}$$

Exchanging the subscripts in Eq. (16a), we have

$$\boldsymbol{K}_b \cdot \begin{Bmatrix} \boldsymbol{U}_i \\ \boldsymbol{U}_j \end{Bmatrix} = \begin{bmatrix} \boldsymbol{F}_i \\ \boldsymbol{F}_j \end{bmatrix} \tag{16c}$$

$\boldsymbol{K}_b$ is the geometric nonlinear stiffness corresponding to accumulative displacements. On considering up till the r-th order terms $\boldsymbol{G}_r$ in Eq. (14), the stiffness matrix with r-order precision is obtained

$$\boldsymbol{K}_b = \boldsymbol{K}_{1,b} + \boldsymbol{K}_{2,b} + \ldots + \boldsymbol{K}_{r,b} \tag{17b}$$

It should be pointed out that the r-order terms in stiffness matrix are proportional to L^{-r}, therefore, the third-order terms and upwards have no obvious influence on the computational precision.

2.1.2 Tangent stiffness matrix for 3-D bar element

In Eq. (16b), the load vector $\boldsymbol{F}$ might as well be rewritten as $\eta \cdot \tilde{\boldsymbol{F}}$, where η is load parameter and $\tilde{\boldsymbol{F}}$ is load mode. If the load system with single load parameter is conservative, $\tilde{\boldsymbol{F}}$ is constant vector. For the convenience of derivation, the matrix $\boldsymbol{K}_b$ can be expressed with a six-dimensional vector $\boldsymbol{e}_k (k = 1, 2, \ldots, 6)$, that is

$$\boldsymbol{K}_b = [\boldsymbol{e}_1 \ \ \boldsymbol{e}_2 \ \ \ldots \ \ \boldsymbol{e}_6] \tag{18}$$

Thus, Eq.(16b) becomes as

$$\boldsymbol{\Phi} = \boldsymbol{e}_1 u_i + \boldsymbol{e}_2 v_i + \boldsymbol{e}_3 w_i + \ldots + \boldsymbol{e}_6 w_j - \eta \cdot \tilde{\boldsymbol{F}} = 0 \tag{19}$$

Differentiating Eq. (19), we have

$$\boldsymbol{K}_{T,b} \cdot \delta \boldsymbol{U} = \delta \eta \cdot \tilde{\boldsymbol{F}} \tag{20}$$

where

$$\boldsymbol{K}_{T,b} = \left[\frac{\partial \boldsymbol{\Phi}}{\partial u_i} \quad \frac{\partial \boldsymbol{\Phi}}{\partial v_i} \quad \ldots \quad \frac{\partial \boldsymbol{\Phi}}{\partial w_j}\right] \tag{21}$$

$$\delta \boldsymbol{U} = [\delta u_i \quad \delta v_i \quad \ldots \quad \delta w_j]^T$$

Noticing that

$$\left.\begin{aligned} \frac{\partial \boldsymbol{\Phi}}{\partial u_i} &= -\frac{\partial \boldsymbol{\Phi}}{\partial u_j} = \boldsymbol{e}_1 - \frac{\partial \boldsymbol{e}_1}{\partial u_i} \cdot \Delta x - \frac{\partial \boldsymbol{e}_2}{\partial u_i} \cdot \Delta y - -\frac{\partial \boldsymbol{e}_3}{\partial u_i} \cdot \Delta z \\ \frac{\partial \boldsymbol{\Phi}}{\partial v_i} &= -\frac{\partial \boldsymbol{\Phi}}{\partial v_j} = \boldsymbol{e}_2 - \frac{\partial \boldsymbol{e}_1}{\partial v_i} \cdot \Delta x - \frac{\partial \boldsymbol{e}_2}{\partial v_i} \cdot \Delta y - \frac{\partial \boldsymbol{e}_3}{\partial v_i} \cdot \Delta z \\ \frac{\partial \boldsymbol{\Phi}}{\partial w_i} &= -\frac{\partial \boldsymbol{\Phi}}{\partial w_j} = \boldsymbol{e}_3 - \frac{\partial \boldsymbol{e}_1}{\partial w_i} \cdot \Delta x - \frac{\partial \boldsymbol{e}_2}{\partial w_i} \cdot \Delta y - \frac{\partial \boldsymbol{e}_3}{\partial w_i} \cdot \Delta z \end{aligned}\right\} \tag{22}$$

then, Eq. (21) can be rewritten in following form

$$\boldsymbol{K}_{T,b} = \begin{bmatrix} \boldsymbol{K}_{t,b} & -\boldsymbol{K}_{t,b} \\ -\boldsymbol{K}_{t,b} & \boldsymbol{K}_{t,b} \end{bmatrix} \tag{23}$$

$$\boldsymbol{K}_{t,b} = \boldsymbol{K}_{t1} + \boldsymbol{K}_{t2}$$

$$\boldsymbol{K}_{t1} = \frac{EA}{L}\begin{bmatrix} l^2 & lm & ln \\ lm & m^2 & mn \\ ln & mn & n^2 \end{bmatrix} \tag{24}$$

$$\boldsymbol{K}_{t2} = \frac{EA}{L^2}\begin{bmatrix} a_{11} & a_{12} & a_{13} \\ & a_{22} & a_{23} \\ symmetry & & a_{33} \end{bmatrix} \tag{25}$$

in which, $\boldsymbol{K}_{T,b}$ is the tangential stiffness matrix of 3-D bar element with second-order precision. The elements in Eq. (25) are expressed as follows

$$\left.\begin{aligned}
a_{11} &= (3l-3l^3)\cdot\Delta x+(m-3l^2m)\cdot\Delta y+(n-3l^2n)\cdot\Delta z\\
a_{12} &= a_{21}=(m-3l^2m)\cdot\Delta x+(l-3lm^2)\cdot\Delta y-3lmn\cdot\Delta z\\
a_{13} &= a_{31}=(n-3l^2n)\cdot\Delta x-3lmn\cdot\Delta y+(l-3\ln^2)\cdot\Delta z\\
a_{22} &= (l-3lm^2)\cdot\Delta x+(3m-3m^3)\cdot\Delta y+(n-3m^2n)\cdot\Delta z\\
a_{23} &= a_{32}=-3lmn\cdot\Delta x+(n-3m^2n)\cdot\Delta y+(m-3mn^2)\cdot\Delta z\\
a_{33} &= (l-3\ln^2)\cdot\Delta x+(m-3mn^2)\cdot\Delta y+(3n-3n^3)\cdot\Delta z
\end{aligned}\right\} \tag{26}$$

where $\Delta x = u_j - u_i,\quad \Delta y = v_j - v_i,\quad \Delta z = w_j - w_i$

2.2 Material nonlinearity of steel tube element

Various steel tubes are widely used to be members for SLS and usually considered as the tension/ compression 3-D bar elements with hinged connection. Let it be supposed that the member movement and deformation is within the extent of large displacement and small strain and the Bauschinger effect for steel tube can be neglected.

The ideal elasto-plastic mechanical model can be used for tension steel tube element, that is,

$$\left.\begin{aligned}
E_t &= E, \quad \text{if} \quad \varepsilon \le \varepsilon_y\\
E_t &= 0, \quad \text{if} \quad \varepsilon > \varepsilon_y
\end{aligned}\right\} \tag{27}$$

and for compression steel tube element, the elasto-plastic model of ultimate points instability is adaptable due to the existence of initial bending, initial eccentricity and initial strain. Besides the single step linear model and step by step linearized model (Smith, E.A. 1984, Smith, E.A. and Smith, G.A. 1981), another mechanical model (Shen *et al.* 1988) based on the analysis of ultimate bearing capacity for steel tube element is also useful, in which the axial deformation modulus and the nonlinear stiffness reduced coefficient are introduced. Let σ and ε be the axial stress and strain of the element, then, the incremental stress-strain relation is given by

$$d\sigma = E_t \cdot d\varepsilon \tag{28}$$

If $\varepsilon \le 4.6\times10^{-4} + 3.5\times10^{-4}(1-\lambda/100)$, the element is under elastic stage

$$E_t = E \tag{29}$$

and if $\varepsilon > 4.6\times10^{-4} + 3.5\times10^{-4}(1-\lambda/100)$, it is under elastio-plastic stage

$$E_t = \beta \cdot E \tag{30}$$

where β is the tangent stiffness reduced coefficient of the compression steel tube element. If $\lambda \le 160$, then

$$\beta = \frac{1000\sum_{i=0}^{3}\sum_{j=0}^{6}\alpha_{ij}^{(1)}\cdot j\cdot\left(\frac{\lambda}{100}-1\right)^i(1000\varepsilon-0.687)^{(j-1)}}{E} \tag{31}$$

and if $\lambda > 160$, then

$$\beta = \frac{1000 \sum_{i=0}^{2} \sum_{j=0}^{6} \alpha_{ij}^{(2)} \cdot j \cdot \left(\frac{\lambda}{180} - 1\right)^{i} (1000\varepsilon - 0.7183)^{(j-1)}}{E} \tag{32}$$

in which, f_y is the yield strength of steel, ε_y is the axial strain when $\sigma = f_y$, and λ is the slenderness ratio of steel tube element. The series of coefficients $\alpha_{ij}^{(1)}$ and $\alpha_{ij}^{(2)}$ can be found in Shen (1988). If an element is under unloading state, the linear-elastic property will be introduced

$$E_t = E$$

In the above Eqs., E and E_t are the Young's modulus and tangent modulus respectively.

3. Non-linearity of cable member

Although it is generally elastic in nature, a cable has unique behavior because of its non-linearity in material and geometric senses. Nonlinear elasticity comes from the change of cable stiffness varying with cable tension, and geometric non-linearity results from the change of cable location and shape if large displacement occurs at both ends of a cable.

Three kinds of methodologies, treating the cable as a bar, the finite element method and treating the cable as an arc, can be used to analyze a cable member. Taking the change of chordwise length of cable into account under the uniformly distributed load perpendicular to the chord and introducing the equivalent elastic modulus, a cable can be treated as a bar member. Multi-node isoparametric element for cable member is adopted in finite element method (John 1988, Chu and Ma 1976, Meek 1991, Krishna 1978), but bulky computations are inevitable. Analytics based on treating the cable as an arc is very helpful to find out the distribution law of internal force and displacement fields, but it has very limited range for application. In this study, the 'bar' method is used and the catenary line is approximately replaced by parabola in practice because of its small sag ratio. For convenience, the load component parallel to the cable chord, and the temperature influence and the stress relaxation of cable member under permanent loads are neglected.

3.1 Equivalent elastic modulus for cable member

For a cable member, as in Fig. 2, l and h are the chordwise length and horizontal projection length, f and α are the sag and the angle between cable and the horizontal plane respectively, and A, E_c and q' are the sectional area, the Young's modulus and uniformly distributed load along the horizontal projection. Only the self-weight of cable member is considered here. The distance between nodes k and j is shortened due to the sag, but lengthened due to the tensile stress. So, under initial state (q_i, σ_i) and non-initial state (q and σ) at any loading incremental step, the changes in chordwise length for a cable member are given by

$$\Delta l_i = \Delta l_{\sigma i} + \Delta l_{qi} = \frac{\sigma_i}{E_c} \cdot l - \frac{1}{24} \cdot \frac{q_i^2 l^3}{\sigma_i^2 A^2} \tag{33}$$

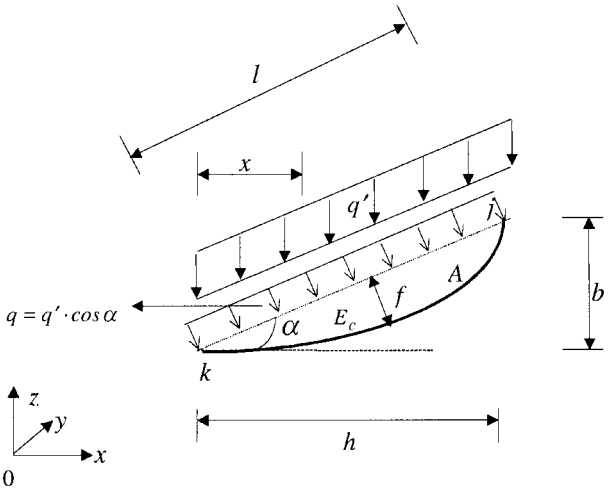

Fig. 2 The schematic diagram of a cable member

$$\Delta l = \frac{\sigma}{E_c} \cdot l - \frac{1}{24} \cdot \frac{q^2 l^3}{\sigma^2 A^2} \tag{34}$$

where σ_i and σ are cable's initial stress and common stress respectively. The increment of chordwise length between the above states is as follows

$$\delta_{kj} = \Delta l - \Delta l_i = -\frac{1}{24}\left(\frac{q^2}{\sigma^2} - \frac{q_i^2}{\sigma_i^2}\right) \cdot \frac{l^3}{A^2} + (\sigma - \sigma_i) \cdot \frac{l}{E_c} \tag{35}$$

paying attention to $q = q_i$, $q = q' \cos\alpha$ and $l = h/\cos\alpha$, and let $\gamma' = q'/A$, the following equation is found from Eq. (35) to be

$$\delta_{kj} = \frac{(\sigma - \sigma_i)}{E_c} \cdot l\left[1 + \frac{E_c \gamma'^2 h^2}{24} \cdot \frac{\sigma + \sigma_i}{\sigma_i^2 \sigma^2}\right] \tag{36}$$

Based on the change of chordwise length between initial and non-initial state in present loading incremental step, the following development is obtained

or
$$E_{eq} = \frac{E_c}{1 + \zeta h^2 \times 10^{-6}} \tag{37}$$

where

$$\zeta = E_c \cdot \frac{\gamma'^2(\sigma_i + \sigma)}{24\sigma_i^2 \sigma^2} \cdot 10^6 \tag{38a}$$

and E_{eq} is the equivalent elastic modulus. Eq. (38a) can be regarded as the secant modulus method for cable member at any loading incremental step. If making $\sigma_i = \sigma$ approximately, we have

$$\zeta = E_c \cdot \frac{\gamma'^2}{12\sigma^3} \cdot 10^6 \tag{38b}$$

Here, Eq. (38b) is, in fact, corresponding to the tangent modulus method at the initial state *i* of the present loading incremental step.

We see from Eq. (37) that E_{eq} decreases with the increment of cable length. For example, if ζ = 10 and *h* are equal to 50 m, 100 m and 200 m respectively, E_{eq}/E_c are equal to 0.976, 0.90 and 0.715. For steel strand cables, ζ usually varies between 2 and 50.

As the above derivation is on the basis of considering a cable as parabola, the results are sure to be in discrepancy with the results obtained from precise computation based on the catenary. Let ERR = $\left|\overline{\delta}/\delta^* - 1\right|$, where δ^* is the exact extension of a cable, and $\overline{\delta}$ is the approximate extension evaluated by using equivalent elastic modulus. It is clear that, through a series of computation, the result based on secant modulus method and precise result fit well. For instance, the ERR is less than 1%, if the cable length is shorter than 400 m. However, the difference between the result based on the tangent modulus method and precise result is not ignored, e.g., the ERR for a cable with the length of 100 m is around 2%. Because cable length in CSLS is much shorter than 400 m for practical applications, it is acceptable that the secant modulus method is regarded as a good approximation.

3.2 Nonlinear equilibrium equation and tangent stiffness matrix for cable member

In the global coordinate systems, let the coordinates of both ends of a cable member connected with a spatial latticed shell and a tower column are (x_i, y_i, z_i) and (x_j, y_j, z_j) respectively. With the displacements of (u_i, v_i, w_i) and (u_j, v_j, w_j) of nodes *i* and *j*, the length and tension increment in cable's chordwise direction is *dl* and *dS* respectively, then

$$dS = \frac{E_{eq} \cdot A}{l'} dl \tag{39}$$

The cable tangent stiffness may be given by

$$k_c = \frac{dS}{dl} = \frac{E_{eq}A}{l'} \tag{40}$$

Substituting Eq. (37) into Eq. (39) with *h* replaced by *h'*, the deploying formulation of cable tangent stiffness can be obtained, where

$$\left.\begin{aligned} h' &= l'\cos\alpha \\ dl &= l' - l \\ l &= \sqrt{(x_j - x_i)^2 + (y_j - y_i)^2 + (z_j - z_i)^2} \\ l' &= \sqrt{[(x_j - x_i) + (u_j - u_i)]^2 + [(y_j - y_i) + (v_j - v_i)]^2 + [(z_j - z_i) + (w_j - w_i)]^2} \end{aligned}\right\} \tag{41}$$

The nonlinear equilibrium equation for cable member under initial global coordinate systems can be expressed as follows

$${}_0^t\boldsymbol{K}_c \cdot \Delta\boldsymbol{U} = {}_0^{t+\Delta t}\boldsymbol{F}_c - \boldsymbol{T}'' \cdot {}_0^t\boldsymbol{S} \tag{42}$$

where

$$ {}_0^t\boldsymbol{K}_c = \boldsymbol{T}''^{\boldsymbol{T}} \cdot \boldsymbol{k}_c \cdot \boldsymbol{T}' \tag{43} $$

$$ \Delta\boldsymbol{U} = [\Delta u_i \;\; \Delta v_i \;\; \Delta w_i \;\; \Delta u_j \;\; \Delta v_j \;\; \Delta w_j] \tag{44} $$

In the above equations, ${}_0^t\boldsymbol{K}_c$ and ${}_0^t\boldsymbol{S}$ are the tangential stiffness matrix and the tension vector of cable member at the time t respectively. ${}_0^{t+\Delta t}\boldsymbol{F}_c$ is the joint load vector at the time $t + \Delta t$. $\Delta\boldsymbol{U}$ is the displacement incremental vector from time t to $t + \Delta t$. The displacement transformation vector $\boldsymbol{T}'$ and the tension transformation vector $\boldsymbol{T}''$ of cable member between the initial and the updated global coordinate systems under the circumstances of large deformation are

$$ \boldsymbol{T}' = [-a'_{ij} \;\; -b'_{ij} \;\; -c'_{ij} \;\; a'_{ij} \;\; b'_{ij} \;\; c'_{ij}]^T \tag{45a} $$

$$ \boldsymbol{T}'' = [-a''_{ij} \;\; -b''_{ij} \;\; -c''_{ij} \;\; a''_{ij} \;\; b''_{ij} \;\; c''_{ij}]^T \tag{45b} $$

where

$$ \left.\begin{aligned} a'_{ij} &= a_{ij} + \frac{u_j - u_i}{2l'} \\ b'_{ij} &= b_{ij} + \frac{v_j - v_i}{2l'} \\ c'_{ij} &= c_{ij} + \frac{w_j - w_i}{2l'} \end{aligned}\right\}, \quad \left.\begin{aligned} a''_{ij} &= a_{ij} + \frac{u_j - u_i}{l'} \\ b''_{ij} &= b_{ij} + \frac{v_j - v_i}{l'} \\ c''_{ij} &= c_{ij} + \frac{w_j - w_i}{l'} \end{aligned}\right\}, \quad \left.\begin{aligned} a_{ij} &= \frac{x_j - x_i}{l} \\ b_{ij} &= \frac{y_j - y_i}{l} \\ c_{ij} &= \frac{z_j - z_i}{l} \end{aligned}\right\} \tag{46} $$

It is apparent from Eqs. (45) and (46) that $\boldsymbol{T}'$ is different from $\boldsymbol{T}''$.

4. Stiffness matrix of tower column

A tower column can be considered as a special 3-D cantilever beam element with double-node or multi-node because of the characteristics of CSLS. For the tower column itself, the connections between sub-elements such as e_l, e_m and e_u in Fig. 3 are rigid. The connections among cable, tower column and main spatial latticed structure, however, should be regarded as pin-connected joints (Dong and Luo 1994).

4.1 The stiffness matrix for tower column with single-layer cables

For a tower column with single-layer of cables (see Fig. 3a), the equilibrium equations based on force method in directions $\bar{x}$ and $\bar{y}$ under LCS are

$$ \boldsymbol{\delta}_{\bar{x}} \cdot \boldsymbol{X} = \boldsymbol{u} \tag{47a} $$

$$ \boldsymbol{\delta}_{\bar{y}} \cdot \boldsymbol{Y} = \boldsymbol{v} \tag{47b} $$

$$ \boldsymbol{\delta}_t = \begin{bmatrix} \delta_{t11} & \delta_{t12} \\ \delta_{t21} & \delta_{t22} \end{bmatrix}, \qquad (t = \bar{x}, \text{ or } \bar{y}) \tag{48} $$

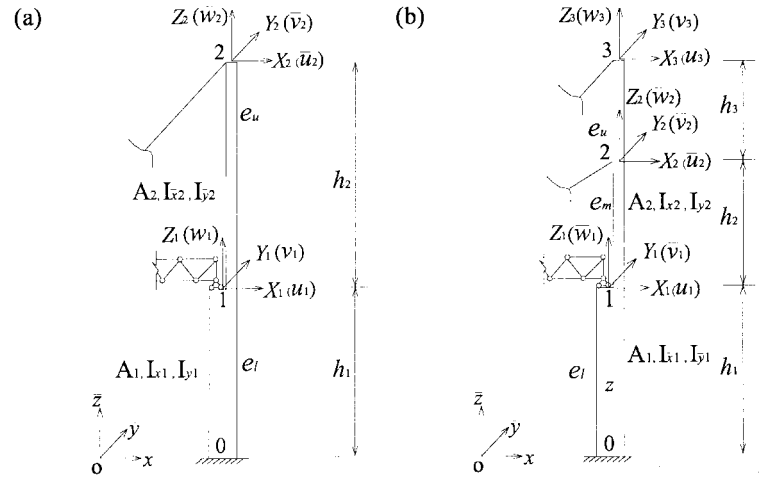

Fig. 3 The drawing of a tower column with cables (under the local coordinate system $o\overline{xyz}$)

$$\boldsymbol{X} = [X_1 \;\; X_2]^T, \qquad \boldsymbol{u} = [\bar{u}_1 \;\; \bar{u}_2]^T \tag{49a}$$

$$\boldsymbol{Y} = [Y_1 \;\; Y_2]^T, \qquad \boldsymbol{v} = [\bar{v}_1 \;\; \bar{v}_2]^T \tag{49b}$$

in which, $\boldsymbol{\delta}_{\bar{x}}$ and $\boldsymbol{\delta}_{\bar{y}}$ are the flexibility matrices for tower column in directions $\bar{x}$ and $\bar{y}$ respectively. The stiffness equation in direction $\bar{x}$ is found from Eq. (47a) to be

$$\boldsymbol{K}_{\bar{x}} \cdot \boldsymbol{u} = \boldsymbol{X} \tag{50}$$

$$\boldsymbol{K}_{\bar{x}} = \delta_{\bar{x}}^{-1} = \begin{bmatrix} K_{\bar{x}11} & K_{\bar{x}12} \\ K_{\bar{x}21} & K_{\bar{x}22} \end{bmatrix} \tag{51}$$

$$\left.\begin{aligned} K_{\bar{x}11} &= \frac{1 + 3\omega + 3\omega^2 + \omega^3/\xi_{\bar{x}}}{\Delta_{\bar{x}}} \cdot \alpha_{\bar{x}} \\ K_{\bar{x}12} &= K_{\bar{x}21} = \frac{1 + \frac{3}{2} \cdot \omega}{\Delta_{\bar{x}}} \cdot \alpha_{\bar{x}} \\ K_{\bar{x}22} &= \frac{\alpha_{\bar{x}}}{\Delta_{\bar{x}}} \\ \Delta_{\bar{x}} &= (1 + 3\omega + 3\omega^2 + \omega^3/\xi_{\bar{x}}) - \left(1 + \frac{3}{2} \cdot \omega\right)^2 \\ \omega &= \frac{h_2}{h_1}, \quad \xi_{\bar{x}} = \frac{I_{\bar{y}2}}{I_{\bar{y}1}}, \quad \alpha_{\bar{x}} = \frac{3EI_{\bar{y}1}}{h_1^3} \end{aligned}\right\} \tag{52}$$

where $\boldsymbol{K}_{\bar{x}}$ is stiffness matrix in direction $\bar{x}$. The stiffness matrix $\boldsymbol{K}_{\bar{y}}$ and $\boldsymbol{K}_{\bar{z}}$ (that is, in directions $\bar{y}$ and $\bar{z}$) can be easily obtained by means of the same process. Assembling these stiffness matrices above, we obtain the stiffness matrix $\overline{\boldsymbol{K}}_{\boldsymbol{tower}}$ for tower column under LCS.

4.2 The stiffness matrix for tower column with double-layer cables

For a tower column with double-layer cables (see Fig. 3b), the equilibrium equations based on force method in directions $\bar{x}$ and $\bar{y}$ under LCS are like Eqs. (47a) and (47b). But Eqs. (49a) and (49b) become

$$\boldsymbol{X} = [X_1 \;\; X_2 \;\; X_3]^T, \qquad \boldsymbol{u} = [\bar{u}_1 \;\; \bar{u}_2 \;\; \bar{u}_3]^T \tag{53a}$$

$$\boldsymbol{Y} = [Y_1 \;\; Y_2 \;\; Y_3]^T, \qquad \boldsymbol{u} = [\bar{v}_1 \;\; \bar{v}_2 \;\; \bar{v}_3]^T \tag{53b}$$

and Eq. (48) also becomes

$$[\delta_t] = \begin{bmatrix} \delta_{t11} & \delta_{t12} & \delta_{t13} \\ & \delta_{t22} & \delta_{t23} \\ symmetry & & \delta_{t33} \end{bmatrix}, \qquad (t = \bar{x}, \quad \text{or} \quad \bar{y}) \tag{54}$$

where

$$\left.\begin{aligned} \delta_{t11} &= \alpha_t, \quad \delta_{t12} = \delta_{t21} = \alpha_t \cdot \left(1 + \frac{3}{2}\omega_1\right) \\ \delta_{t22} &= \alpha_t \cdot [1 + 3\omega_1 + 3\omega_1^2 + \omega_1^3/\xi_t] \\ \delta_{t13} &= \delta_{t31} = \alpha_t\left[1 + \frac{3}{2}\omega_4\right] \\ \delta_{t23} &= \delta_{t32} = \alpha_t\left(1 + \frac{3}{2}\omega_3\right) \cdot \omega_1^3/\xi_t + \alpha_t \cdot (1 + 3\omega_5 + 3\omega_1\omega_4) \\ \delta_{t33} &= \alpha_t(1 + \omega_3)^3 \cdot \omega_1^3/\xi_t + \alpha_t[1 + 3(\omega_1 + \omega_2)(1 + \omega_1 + \omega_2)] \end{aligned}\right\} \tag{55}$$

$$\left.\begin{aligned} \alpha_t &= \frac{h_1^3}{3EI_{t1}}, \quad \xi_t = \frac{I_{t2}}{I_{t1}} \\ \omega_1 &= \frac{h_2}{h_1}, \quad \omega_2 = \frac{h_3}{h_1}, \quad \omega_3 = \frac{h_3}{h_2} \\ \omega_4 &= \omega_1 + \omega_2, \quad \omega_5 = \omega_1 + \frac{\omega_2}{2} \end{aligned}\right\} \tag{56}$$

Substituting Eq. (54) into Eq. (47a) or (47b), and inverting the matrices $\boldsymbol{\delta}_{\bar{x}}$ and $\boldsymbol{\delta}_{\bar{y}}$, the stiffness matrices $\boldsymbol{K}_{\bar{x}}$ and $\boldsymbol{K}_{\bar{y}}$ in directions $\bar{x}$ and $\bar{y}$ under LCS can be obtained. Moreover, the stiffness

matrix $\boldsymbol{K}_{\bar{z}}$ in direction $\bar{z}$ is obtained easily by use of matrix-displacement method. The stiffness equation for tower column under LCS is given by

$$\bar{\boldsymbol{K}}_{tower} \cdot \boldsymbol{\delta} = \boldsymbol{F}_t \tag{57}$$

in which

$$\delta = [\bar{u}_1 \ \bar{v}_1 \ \bar{w}_1 \ \bar{u}_2 \ \bar{v}_2 \ \bar{w}_2 \ \bar{u}_3 \ \bar{v}_3 \ \bar{w}_3]^T$$
$$\boldsymbol{F}_t = [X_1 \ Y_1 \ Z_1 \ X_2 \ Y_2 \ Z_2 \ X_3 \ Y_3 \ Z_3]^T$$

$$\bar{\boldsymbol{K}}_{tower} = \begin{bmatrix} K_{\bar{x}11} & 0 & 0 & K_{\bar{x}12} & 0 & 0 & K_{\bar{x}13} & 0 & 0 \\ & K_{\bar{y}11} & 0 & 0 & K_{\bar{y}12} & 0 & 0 & K_{\bar{y}13} & 0 \\ & & K_{\bar{z}11} & 0 & 0 & K_{\bar{z}12} & 0 & 0 & K_{\bar{z}13} \\ & & & K_{\bar{x}22} & 0 & 0 & K_{\bar{x}23} & 0 & 0 \\ & & & & K_{\bar{y}22} & 0 & 0 & K_{\bar{y}23} & 0 \\ & & & & & K_{\bar{z}22} & 0 & 0 & K_{\bar{z}23} \\ & & \textit{symmetry} & & & & K_{\bar{x}33} & 0 & 0 \\ & & & & & & & K_{\bar{y}33} & 0 \\ & & & & & & & & K_{\bar{z}33} \end{bmatrix} \tag{58}$$

5. Nonlinear seismic responses

As above statement, CSLS consists of 3-D bar element, cable member and tower column member. Once the stiffness matrix, mass matrix and damping matrix of each member of a cable-stayed spatial latticed structure are assembled, the structural nonlinear dynamic equation can be obtained. The dynamic equation at time step $i + 1$ (that is, $t + \Delta t$) can be expressed as

$$\boldsymbol{M} \cdot \ddot{\boldsymbol{u}}_{i+1} + \boldsymbol{C}_{i+1} \cdot \dot{\boldsymbol{u}}_{i+1} + \boldsymbol{R}_{i+1} = -\boldsymbol{M} \cdot \boldsymbol{N} \cdot \ddot{\boldsymbol{u}}_{g,\,i+1} \tag{59a}$$

After linearization, the incremental dynamic equation is

$$\boldsymbol{M} \cdot \ddot{\boldsymbol{u}}_{i+1} + \boldsymbol{C}_{i+1} \cdot \dot{\boldsymbol{u}}_{i+1} + \boldsymbol{K}_{T,\,i} \cdot \Delta \boldsymbol{u}_{i+1} = -\boldsymbol{M} \cdot \boldsymbol{N} \cdot \ddot{\boldsymbol{u}}_{g,\,i+1} - \boldsymbol{R}_i \tag{59}$$
$$\boldsymbol{R}_{i+1} = \boldsymbol{R}_i + \boldsymbol{K}_{T,\,i} \cdot \Delta \boldsymbol{u}_{i+1}$$

where $\dot{\boldsymbol{u}}_{i+1}$, $\ddot{\boldsymbol{u}}_{i+1}$ and $\ddot{\boldsymbol{u}}_{g,\,i+1}$ are velocity, structural acceleration and seismic acceleration vector at time step $i + 1$ respectively. $\Delta \boldsymbol{u}_{i+1}$, $\boldsymbol{K}_{T,\,i}$, and $\boldsymbol{R}_i$ are the incremental displacement vector from time step i to $i + 1$, the structural tangential stiffness matrix and nodal force vector at time step i. $\boldsymbol{M}$ is the structural mass matrix and $\boldsymbol{C}$ is damping matrix. And

$$\boldsymbol{N} = [\boldsymbol{N}_x \ \boldsymbol{N}_y \ \boldsymbol{N}_z]$$

$$\left.\begin{aligned} \boldsymbol{N}_x &= [1\ 0\ 0\ 1\ 0\ 0\ \ldots\ 1\ 0\ 0]^T \\ \boldsymbol{N}_y &= [0\ 1\ 0\ 0\ 1\ 0\ \ldots\ 0\ 1\ 0]^T \\ \boldsymbol{N}_x &= [0\ 0\ 1\ 0\ 0\ 1\ \ldots\ 0\ 0\ 1]^T \end{aligned}\right\}$$

The dynamic incremental equation above can be solved by Newmark method (Newmark 1959). To avoid the error accumulation, however, an iteration procedure is added at each time step. That is, if $\Delta \boldsymbol{u}_{i+1}^{(k-1)}$ are obtained from Eq. (59b) by use of Newmark method, we have

$$\boldsymbol{u}_{i+1}^{k-1} = \boldsymbol{u}_i + \Delta \boldsymbol{u}_{i+1}^{(k-1)} \tag{60}$$

where $\boldsymbol{u}_i$ is displacement vector at time step i and $\boldsymbol{u}_{i+1}^{k-1}$ is the (k-1)th iteration displacement vector at time step $i + 1$.

Making use of $\boldsymbol{u}_{i+1}^{k-1}$, we recalculate $\boldsymbol{R} = \boldsymbol{R}_{i+1}^{k-1}$. Also, the linearization is introduced again

$$\boldsymbol{R}_{i+1} = \boldsymbol{R}_{i+1}^{k-1} + \boldsymbol{K}_{T,i} \cdot \Delta \boldsymbol{u}_{i+1}^{\prime\, k} \tag{61}$$

where

$$\Delta \boldsymbol{u}_{i+1}^{\prime\, k} = \Delta \boldsymbol{u}_{i+1}^{k} - \Delta \boldsymbol{u}_{i+1}^{k-1} \tag{62}$$

Eq. (62) is the correction for $\Delta \boldsymbol{u}_{i+1}^{k-1}$. The fundamental equation for the k-th iteration is given by

$$\boldsymbol{M} \cdot \ddot{\boldsymbol{u}}_{i+1}^{k-1} + \boldsymbol{C} \cdot \dot{\boldsymbol{u}}_{i+1}^{k-1} + \boldsymbol{K}_{T,i} \cdot \Delta \boldsymbol{u}_{i+1}^{\prime\, k} = \tilde{\boldsymbol{R}}_{i+1} - \boldsymbol{R}_{i+1}^{k-1} \tag{63}$$

where

$$\tilde{\boldsymbol{R}}_{i+1} = -\boldsymbol{M} \cdot \boldsymbol{N} \cdot \ddot{\boldsymbol{u}}_{g,i+1}$$

In Eq. (63), $\ddot{\boldsymbol{u}}_{i+1}^{k-1}$ and $\dot{\boldsymbol{u}}_{i+1}^{k-1}$ are the acceleration and velocity vector obtained by use of $\Delta \boldsymbol{u}_{i+1}^{k-1}$ by virtue of Newmark method. From Eq. (62), we have

$$\Delta \boldsymbol{u}_{i+1}^{k} = \Delta \boldsymbol{u}_{i+1}^{k-1} + \Delta \boldsymbol{u}_{i+1}^{\prime\, k}$$

Substituting $\Delta \boldsymbol{u}_{i+1}^{k}$ obtained from above process into Eq. (60), the next iteration is proceeded. The iteration process ends when $\Delta \boldsymbol{u}_{i+1}^{\prime}$ is small enough.

6. Examples and their analyses

Based on the above theories and methods, the numerical studies are focused on such aspects as the ultimate load carrying capacity and the nonlinear seismic responses of CSLS. The influences of some geometrical and physical factors upon structural behavior are also investigated.

Table 1 Ultimate load carrying capacities of cable-stayed double layer spatial latticed dome and their comparisons

No.	working mode	ultimate load carrying capacity (kN)
1	without cables and elastic supports system considered	15.05
2	with cables, elastic supports system considered and the deflection of tower columns neglected	23.80
3	with cables, rigid supports system considered and the deflection of tower columns neglected	29.07
4	with cables, elastic supports system and the deflection of tower columns considered	21.13

Note: the spring stiffness of elastic supports in Table 1 is $k = 5.0 \times 10^4$ kN/m

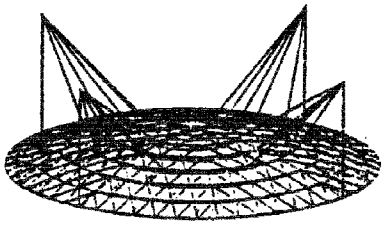

(a) the schematic diagram of cable-stayed double layer dome of type K8-7

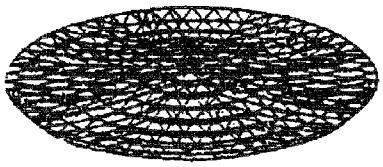

(b) structural deflection under mode 1

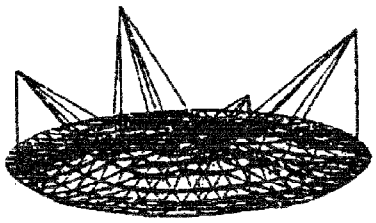

(c) structural deflection under mode 2

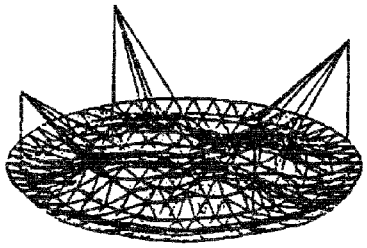

(d) structural deflection under mode 3

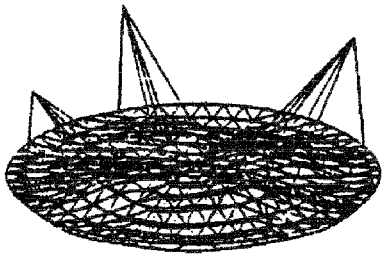

(e) structural deflection under mode 4

Fig. 4 The structural schematic diagram and the deflection shapes at ultimate state of the dome

6.1 Ultimate load carrying capacities of cable-stayed spatial latticed dome and their comparisons

Fig. 4(a) shows a cable-stayed double layer spatial latticed dome whose top layer and lower layer are constituted by the configuration with the Keiwitt 8-7 grid and honeycomb grid respectively (briefly called as cable-stayed double layer dome of type K8-7). This dome has a number of grids of 16 × 10, a span of 80.0 m and arch rise of 8.0 m. Its upper chord joints are anchored on the outer annular beam, which form the bearing supports system. Four tower columns are set up at four intersections between the outer annular beam and far ends of the two main orthogonal ribs of this dome. Each tower column tying in with five cables is made up of upper and lower parts with the length of 25.0 m and 10.0 m respectively. The uniform load system is exerted on the upper chords' joints.

Nonlinear static computation is carried out to study the structural behavior under different working modes. The results of ultimate load carrying capacities are shown in Table 1. It is clear that the ultimate load carrying capacities of the dome under working mode 2, 3 and 4 enhance by 58.15%, 93.17% and 40.4% compared with that under working mode 1 respectively. The result under mode 2 is 81.9% only of that under mode 3, while under mode 4 it reduces by 12.6% compared with under mode 2. The computations based on elastic supports system obviously differ from those based on rigid supports system. Those based on the latter tend to be unsafe, because of the overestimation of load carrying capacity of the structure. Fig. 4(b)~(e) show the deflections of these modes at the moment of ultimate load respectively. It can be found that the deflection of spatial latticed dome with cables notably abates, in other words, the dome stiffness improves greatly. The numerical results also show that the improvement of structural strength and stiffness of CSLS is relevant not only to cables, but also to tower columns. In addition, there is evident difference between the computations based on whether or not the deflection of tower columns is considered.

6.2 Nonlinear seismic responses

A series of computations is carried out for the dome shown in Fig. 4(a), which is subjected to El-Centro and Taft seismic wave records in directions x, y and z at the same time. In Eq. (59b), the lumped mass matrix and the Rayleigh damping matrix are introduced (Clough and Penzien 1975), and the cables are supposed to keep in tensile state during the period of the seismic wave's time history. The damping ratio 2% of the basic mode of vibration is used. The displacement time histories (DTH) of two typical nodes (named as node 1 and 2) of the dome subjected to El-Centro wave records are showed in Figs. 5(a), (b) and Figs. 6(a), (b). Those subjected to Taft wave records are showed in Figs. 7(a), (b) and Figs. 8(a), (b). It is very clear from the figures that structural responses of CSLS are less than those of CLS greatly, the vertical seismic responses of both CSLS and CLS are obviously greater than the horizontal ones and the configuration of displacement time history curve of one node is very different from that of another node. It can be found that, under the same seismic wave records acting on the dome, the peak values of DTH of different joints appear at different moments. The velocity and acceleration time histories of both structures have the similar phenomena above. Therefore, it can be deduced that the internal force peak values of different members in structures occur at different moments.

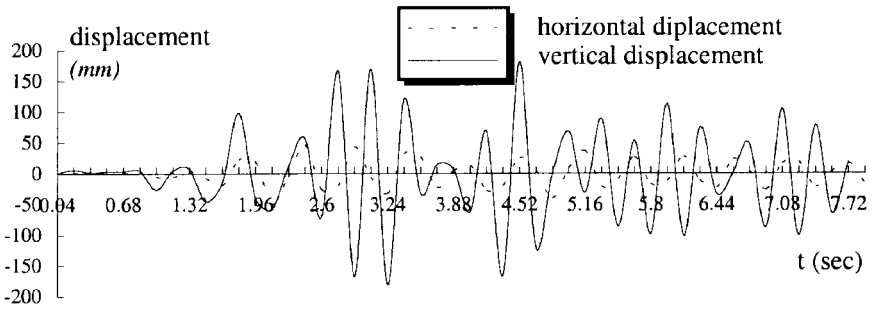

(a) time-displacement curve of node 1

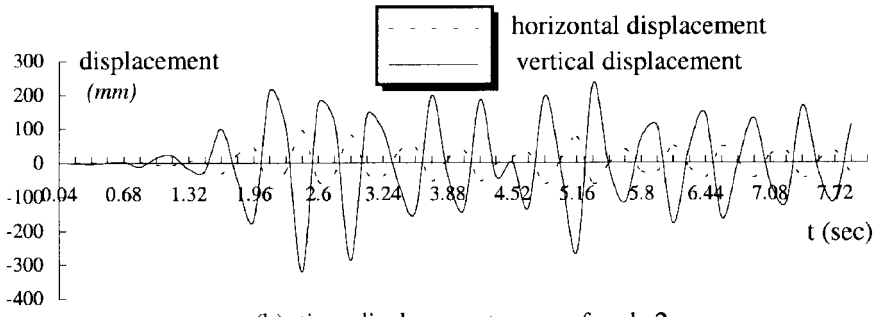

(b) time-displacement curve of node 2

Fig. 5 Displacement time history of double layer dome of type K8-7 under El-Centro seismic wave records

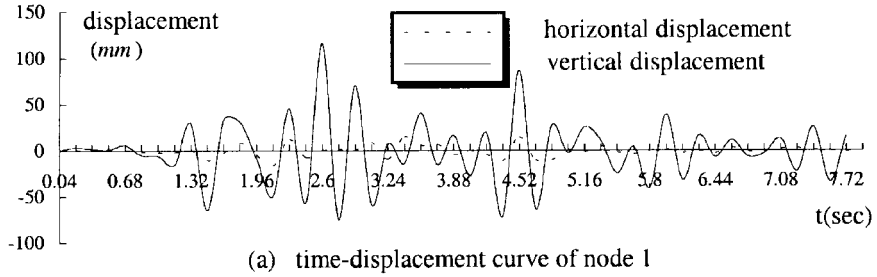

(a) time-displacement curve of node 1

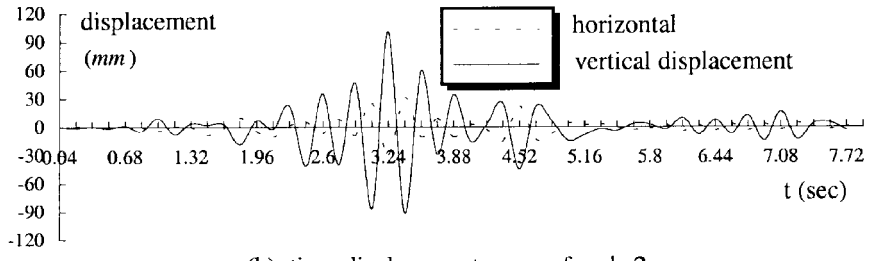

(b) time-displacement curve of node 2

Fig. 6 Displacement time history of cable-stayed double layer dome of type K8-7 under El-Centro seismic wave records

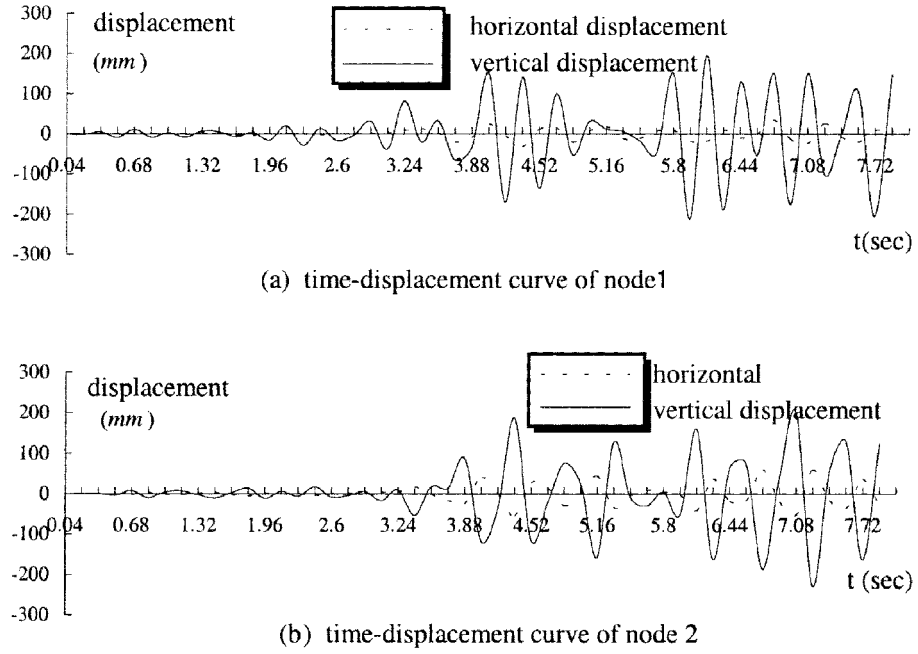

Fig. 7 Displacement time history of double layer dome of type K8-7 under Taft seismic wave records

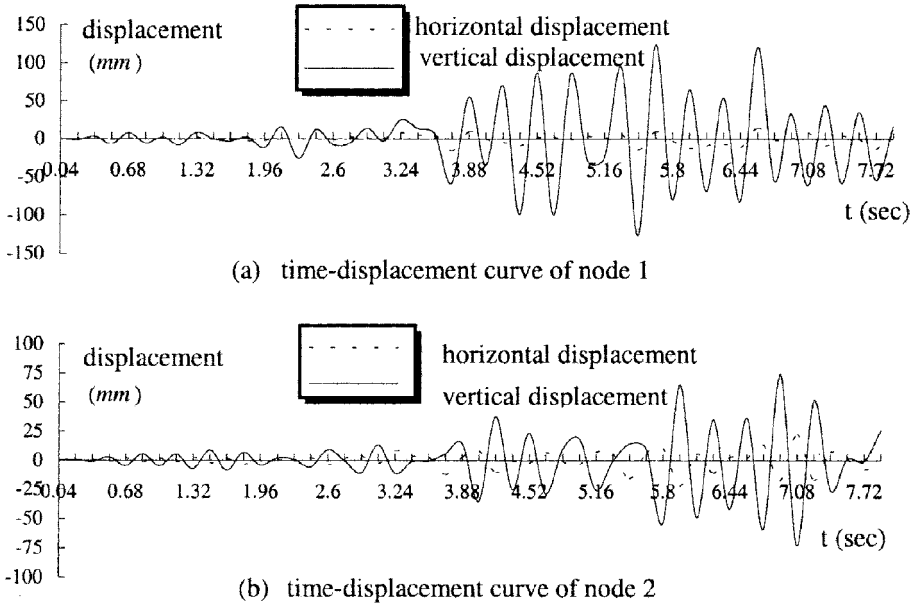

Fig. 8 Displacement time history of cable-stayed double layer dome of type K8-7 under Taft seismic wave records

7. Conclusions

This paper focuses attention on the nonlinear analysis of long-span CSLS. Based on the variation principle, a novel geometric nonlinear formulation for 3-D bar element considering large displacement and infinitesimal rotation increments with the precision of second-order is developed. Theoretically, tangent stiffness formulation with any order of precision can be obtained by use of this method. The cable nonlinearity is discussed and the investigation shows that the secant modulus method for cable member can be considered as a reasonably exact method and the tangent modulus method may be used in approximate computation. Considering the tower column to which cables link, as a special kind of beam element, a new simplified stiffness formulation is developed. In this study, the computational strategies for the nonlinear dynamic response of structures are investigated, and the ultimate load carrying capacities and structural nonlinear seismic responses are analyzed numerically. It is very clear from computations that the ultimate load carrying capacities and stiffness of CSLS (that is, SLS with cables) enhance significantly. It is shown that structural seismic responses of CSLS are less than those of CLS greatly, the vertical responses of both CSLS and CLS are obviously greater than the horizontal ones and the configuration of displacement time history curve of one node is very different from that of another node. The study also points out that the stiffness of tower column influences the performance of CSLS to a certain extent and the improvement of structural strength and stiffness of CSLS is relevant not only to cables but also to tower columns. Moreover, obvious difference between the static computations based on the elastic and rigid supports systems exists. The results based on the former should be adopted, while those based on the latter tend to be unsafe due to the overestimation of load carrying capacity.

Acknowledgements

Support from the National Natural Science Foundation of China (Project No. 50278054) is acknowledged.

References

Abrate, S. and Sun, C.T. (1983), "Dynamic analysis of geometrically nonlinear truss structures", *Comput. Struct.*, **17**(4), 491-497.

Borri, C. and Hufendiek, H.W. (1985), "Geometrically non-linear behavior of space beam structures", *J. Structural Mechanics*, **13**(1), 1-26.

Buchholdt, H.A. (1999), *An Introduction to Cable Roof Structures*, 2nd ed., Thomas Telford.

Chan, S.L. (1992), "Large deflection kinematic formulations for three-dimensional framed structures", *Comput. Method. Appl. Mech. Eng.*, **95**(1), 17-36.

Chu, Kuang-Han and Ma, David Chia-Chiun (1976), "Nonlinear cable and frame interaction", *J. Struct. Div.*, **102**(ST3), 569-589.

Clough, R.W. and Penzien, J. (1975), *Dynamics of Structures*, McGraw-Hill Inc.

Dong, S.L., Zhao, Y. and Zhou, D. (2000), "New structural forms and new technologies in the development of steel space structures in China", *Advances in Structural Engineering*, **3**(1), 49-65.

Dong, S.L. and Luo, Y.Z. (1994), "The simplified method of cable-stayed space truss analysis (in Chinese)", *Symposiums on New Space Structures*, Zhejiang University Press, Huangzhou, China, 89-92.

Hangai, Y. (1981), "Application of the generalized inverse to the geometrically nonlinear problem", *Solid*

Mechanics Archives, **6**(1), 129-165.
Hobbs, R.E. and Raoof, M. (1996), "Behaviour of cables under dynamic or repeated loading", *J. Construct. Steel Res.*, **39**(1), 31-50.
Hsiao, K.M. and Chang, M.T. (1991), "A motion process for large displacement analysis of spatial frames", *Int. J. Space Structures*, **6**(2), 133-139.
John, W. Leonard (1988), *Tension Structures*, McGraw-Hill Inc., New York.
Kato, S. and Niho, Y. (2000), "Proportioning method for single layer reticulated domes-knock-down factor for proportioning method and estimating ultimate loads", *Proc. Sixth Asian Pacific Conference on Shell and Spatial Structures*, Seoul, **1**, 189-198.
Kato, S., Yamashita, T. and Ueki, T. (2000), "Evaluation of elasto-plastic buckling strength of two-way grid shells using continuum analogy", *Proc. Sixth Asian Pacific Conference on Shell and Spatial Structures*, Seoul, **1**, 105-114.
Kato, S., Ueki, T. and Mukaiyama, Y. (1997), "Study of dynamic collapse of single layer reticular domes subjected to earthquake motion and the estimation of statically equivalent seismic forces", *Int. J. Space Structures*, **12**(3,4), 191-203.
Kato, S. and Mukaiyama, Y. (1995), "Study on dynamic behavior and collapse acceleration of single layer reticular domes subjected to horizontal and vertical earthquake motions", *J. Structural and Construction Engineering*, **77**(4), 87-96.
Kim, Jong-Hwa and Chang, Sung-Pil (2001), "Dynamic stiffness matrix of an inclined cable", *Eng. Struct.*, **23**(12), 1614-1621.
Kneen, P. (1993), "Cable-supported space frame roof structures", *Space Structure 4*, **2**,Thomas Telford, London.
Krishna, Prem (1978), *Cable-Suspended Roofs*, McGraw-Hill Book Inc.
Krishna, P. (2001), "Tension roofs and bridges", *J. Construct. Steel Res.*, **57**(11), 1123-1140.
Liew, J.Y.R., Punniyakotty, N.M. and Shanmugam, N.E. (1997), "Advanced analysis and design of spatial structures", *J. Construct. Steel Res.*, **42**(1), 21-48.
Makowski, Z.S. (1993), "Space structures - a review of the developments within the last decade", *Space Structure 4*, **1**, Thomas Telford, London.
Meek, J.L. (1991), *Computer Methods in Structural Analysis*, E & FN SPON, London.
Narayanan, G. and Krishnamoorthy, C.S. (1990), "An investigation of geometric non-linear formulation for 3D beam element", *Int. J. Nonlinear Mechanics*, **25**(6), 643-662.
Newmark, N.M. (1959), "A method of computation for structural dynamic", *J. Eng. Mech. Div.*, ASCE, **85**, 67-94.
Osamu Hosozawa, Kouhei Shimamura and Taro Mizutani (1999), "The role of cables in large span spatial structures: introduction of recent space structures with cables in Japan", *Eng. Struct.*, **21**(8),795-804.
Schueler, W. (1983), *Horizontal-Span Building Structures*, John Wiley and Sons, New York.
Schrefler, B.A. and Odorizz, S. (1983), "A total lagrangian geometrically nonlinear analysis of combined beam and cable structures", *Comput. Struct.*, **17**(1), 115-127.
Shen, Z.Y., Chen, Y.J. and Chen, X.C. (1988), "Mechanical model of ultimate bearing capacity of steel tube structures (in Chinese)", *J. Tongji University*, **16**(3), 279-292.
Smith, E.A. (1984), "Space trusses nonlinear analysis", *J. Struct. Eng.*, ASCE, **109**(7), 1635-1647.
Smith, E.A. and Smith, G.A. (1981), "Collapes analysis of space trusses", *Proc. of Symposium on Long Span Roof Structures*, ASCE, 127-148.
Starossek, U. (1991), "Dynamic stiffness matrix of sagging cable", *J. Eng. Mech.*, ASCE, **117**(12), 2815-2829.
Yamashita, Tetsuo and Kato, Shiro (2001), "Elastic buckling characteristics of two-way grid shells of single layer and its application in design to evaluate the non-linear behavior and ultimate strength", *J. Construct. Steel Res.*, **57**(12), 1289-1308.